Atmospheric Oxidation of Fluorinated Ethers, E143a (CF_3OCH_3), E134 (CHF_2OCHF_2), and E125 (CHF_2OCF_3)

David A. Good, Mike Kamboures, Randy Santiano, and Joseph S. Francisco*

Department of Chemistry and Department of Earth and Atmospheric Sciences, Purdue University, West Lafayette, Indiana 47907

Received: June 16, 1999; In Final Form: August 31, 1999

The atmospheric oxidation mechanisms of E143a (CF_3OCH_3), E134 (CHF_2OCHF_2), and E125 (CHF_2OCF_3) have been investigated using experimental and ab initio methodology. The oxidation of E143a produces the stable reservoir species trifluoromethyl formate, CF_3OCOH, which further oxidizes to CF_2O and CO_2. Oxidation of E134 and E125 shows the presence of only CF_2O under the condition of high O_2 concentrations. Carbonyl fluoride can be formed from two competing pathways involving the halogenated alkyl radicals formed from hydrogen abstraction of E134 and E125. CO bond fission reactions and O_2 addition reactions compete to produce carbonyl fluoride and a CF_xH_{3-x} radical fragment. Computational modeling of the reaction pathways provides insight into the molecular steps of the degradation process.

I. Introduction

Because of the ability of chlorofluorocarbons (CFCs) to deplete stratospheric ozone, many applications have begun to employ hydrofluorocarbons (HFCs) as working fluids. HFCs contain no chlorine and are thus given ozone depletion potentials of essentially zero. Attention is now focused on global warming, with the goal of reducing greenhouse gas emissions. Air conditioners, heat pumps, and refrigeration devices that use refrigerants also use energy. They contribute to global warming both by the release of the refrigerant and by the emission of carbon dioxide and other greenhouse gases in powering the devices.[1] Some HFCs have fairly significant global warming potentials.[2,3] Leading CFC replacements, such as HFC-125 (CHF_2OCF_3), HFC-134a (CHF_2OCHF_2), and HFC-143a (CF_3OCH_3), have global warming potentials not much lower than the CFCs they replace.[2] In fact, many of the hydrochlorofluorocarbons (HCFCs) would be better replacements than HFCs from a climate-forcing perspective. This situation in combination with the indirect global warming effect resulting from differences in the efficiencies of these systems results in an issue concerning the use of many HFCs and their impact on climate. For this reason, research is still devoted to the exploration of novel, third-generation CFC alternatives.

One such third-generation CFC alternative is the fluorinated ether series. These species are analogous to HFCs with the addition of an ether linkage. The U.S. Environmental Protection Agency (EPA) developed a list of 37 candidate compounds proposed for use as working fluids, 13 of which were fluorinated ethers. The list was narrowed down to 11 species, included CF_3OCH_3 and CHF_2OCF_3.[4−6]

Cooper et al.,[7] using ab initio and semiempirical methods, estimated the energy of the highest occupied molecular orbital, which is then proportional to the rate of reaction with the hydroxyl radical. Using this methodology, atmospheric lifetimes for fluorinated derivatives of dimethyl ether were found to range from 7.3 days (CH_3OCH_2F) to 85 days (CHF_2OCF_3).[7]

In 1992, Zhang et al.[8] measured the rate of reaction of fluorinated ethers with hydroxyl radical using a flash photolysis resonance fluorescence technique. E143a, E134, and E125 were found to have rate constants of 2.14×10^{-14}, 2.53×10^{-14}, and 3.38×10^{-15} cm^3 molecule^{-1} s^{-1}. Lifetimes on the order of 3.0, 2.6, and 19 years, respectively, were calculated.[8] Garland et al.[9] in 1993 measured the rate of reaction of OH radicals with E134 using pump and probe laser-induced fluorescence of OH. A rate expression of $5.4 \times 10^{-13}\, e^{-1560/T}$ was determined. At 298 K the rate was $3.0 \pm 0.7 \times 10^{-15}$ cm^3 molecule^{-1} s^{-1}. A lifetime on the order of 24 years was determined.[9] Huie et al. measured the rate of E134 reaction with OH and determined the 298 K rate constant to be 5.1×10^{-15} cm^3 molecule^{-1} s^{-1} (reported by Garland et al.[9]). Hsu et al.[10] used a relative rate technique to measure the OH rate constants of E143a, E134, and E125 to be $1.9 \times 10^{-12}\, e^{-1555/T}$, $1.9 \times 10^{-12}\, e^{-2006/T}$, and $4.7 \times 10^{-13}\, e^{-2095/T}$, respectively. The 298 K rate constants are thus 1.03×10^{-14}, 2.27×10^{-15}, and 4.16×10^{-16} cm^3 molecule^{-1} s^{-1}, respectively. For E134, the results of Garland, Huie, and Hsu are in reasonable agreement.[9,10] Good et al.,[11] using a two-dimensional (2D) chemical transport model and the rate data of Hsu et al.,[10] determined the lifetimes of E143a, E134, and E125 to be 5.7, 29.0, and 165.0 years, respectively. These results suggest that these ethers have much longer atmospheric lifetimes than previously suspected and that penetration of these ethers into the stratosphere is possible.[11]

One issue that has not been addressed is the atmospheric fate of these hydrofluoroethers (HFEs) after the initial hydrogen abstraction reaction by the hydroxyl radical. Only one investigation has reported on the atmospheric fate of E143a.[28] It is the purpose of this work to examine the atmospheric oxidation products of E143a (CF_3OCH_3), E134 (CHF_2OCHF_2), and E125 (CHF_2OCF_3).

II. Methodology

A. Computational Methods. All calculations were performed with the GAUSSIAN 94 package of programs.[12] Geometry optimizations for all species were carried out for all structures to better than 0.001 Å for bond lengths and 0.1° for angles. The geometries were fully optimized, and a frequency calculation was performed with these geometries. Optimizations were performed with the Becke nonlocal three-parameter exchange

10.1021/jp991979h CCC: $18.00
Published on Web 10/30/1999

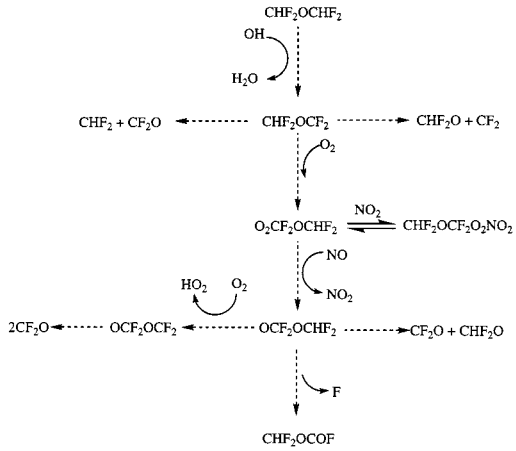

Figure 1. Oxidation mechanism for CHF_2OCHF_2 (E134).

and correlation functional with the Lee−Yang−Parr correctional functional method (B3LYP).[13] The B3LYP optimizations were performed with the medium size 6-31G(d) basis set. In addition, single-point energy calculations were performed using the 6-311+G(2d,2p) basis set. Restricted wave functions were used for closed-shell and unrestricted wave functions for open-shell systems with all orbitals active. The total energies are corrected to 0 K by adding the zero-point energy to the predicted total energy. To obtain the energy at 298 K, the thermal energy of each species is added to its total energy instead of the zero-point energy.

B. Experimental Methods. The experiment consists of a Matteson Instruments Galaxy Series Fourier transform infrared (FTIR) spectrometer operating at 1.0 cm^{-1} resolution in which 64 scans are co-added. The spectrometer uses a KBr beam splitter and a mercury cadmium telluride (MCT) detector capable of operating between 400 and 6600 wavenumbers. The spectrometer is interfaced to a 64 cm^3 Teflon reaction vessel to which gas mixtures of each ether (1 Torr), chlorine (1−2 Torr), and O_2 (0−100 Torr) were added such that the total pressure within the cell remained at 100 Torr. Perpendicular to the IR probe axis is a Lambda Physik Compex 102 excimer laser that was used to initiate the photolysis of molecular chlorine into chlorine atoms (reaction 1). The laser produces 60 mJ of 351 nm radiation while operating at 15 Hz.

$$Cl_2 + h\nu(351\ nm) \rightarrow 2Cl \qquad (1)$$

Reaction mixtures as monitored by their pressures using MKS capacitance manometers were introduced into the chamber and allowed to equilibrate for ~1 h. After photolysis initiation, the reaction was monitored by following IR absorption features from both reactants and products. E134 (1,1,2,2-tetrafluorodimethyl ether, 97.0%) was obtained from Oakwood Products. E125 and E143a were obtained from DuPont Inc. No impurities were detected by gas chromatography/mass spectroscopy (GC/MS), and all reagents were used without further purification.

III. Results and Discussion

A. CHF_2OCHF_2. The oxidation mechanism of E134 is illustrated in Figure 1, and the energetics of all reactions are illustrated and tabulated in Figure 2 and Table 1, respectively. The hydrogen abstraction reaction (reaction 2) is estimated to have a barrier height of 0.8 kcal mol^{-1} at the B3LYP/6-311+G(2d,2p)//B3LYP/6-31G(d) level of theory.

$$CHF_2OCHF_2 + OH \rightarrow CHF_2OCF_2 + H_2O \qquad (2)$$

Hsu et al.,[10] using a relative rate technique, measured the activation barrier to be 4.0 kcal mol^{-1}, which is 3.2 kcal mol^{-1} higher than our calculated activation barrier. This comparison allows for an estimation of the errors associated with our computational methodology.

In Table 1, the enthalpy for reaction 2 is estimated to be −13.8 kcal mol^{-1}. Hsu et al.[10] determined the CH bond dissociation energy of E134 to be 104.0 ± 1.0 kcal mol^{-1} based on observed trends between the CH bond strength of a molecule and its rate of reaction with hydroxyl radical. Given that the OH bond strength of water is 119.3 ± 1.0 kcal mol^{-1}, the enthalpy of reaction 2 can be determined from the CH bond strength of the ether and the OH bond strength of water. Thus, the 298 K enthalpy of reaction 2 is derived from this experimental data to be −15.3 ± 1.4 kcal mol^{-1}. This value compares reasonably well with our ab initio results, which indicate a reaction enthalpy of −13.8 kcal mol^{-1}.

The CHF_2OCF_2 radical formed in the initial hydrogen abstraction reaction can participate in either an oxygen addition or two CO bond dissociation reactions.

$$CHF_2OCF_2 + O_2 \rightarrow CHF_2OCF_2O_2 \qquad (3)$$

$$CHF_2OCF_2 \rightarrow CHF_2O + CF_2 \qquad (4)$$

$$CHF_2OCF_2 \rightarrow CHF_2 + CF_2O \qquad (5)$$

The O_2 addition reaction proceeds without barrier, is exothermic by −30.7 kcal mol^{-1}, and has a negative entropy change of approximately −0.0403 kcal mol^{-1} K^{-1}. The reaction is thus spontaneous by −18.7 kcal mol^{-1} at 298 K. The CO bond-cleaving reaction producing CHF_2O and CF_2 is highly endothermic (56.7 kcal mol^{-1}) and is unlikely to be of any significance at atmospheric temperatures. The CO bond-cleaving reaction producing carbonyl fluoride and CHF_2 is predicted to be exothermic by −1.7 kcal mol^{-1}. In addition a favorable entropy change of 0.0397 kcal mol^{-1} K^{-1} results in a spontaneous process by −13.5 kcal mol^{-1}. Thus, the thermodynamics of reactions 3 and 5 are comparable. Although the thermodynamics for reactions 3 and 5 are similar, the kinetics may not be. The barrier for reaction 5 was found to be 17.5 kcal mol^{-1}, whereas the O_2 addition reaction proceeds without barrier. This result suggests that the bond fission reaction may be slow in comparison with the O_2 addition reaction.

The alkylperoxyl radical formed in reaction 3 reacts with NO under atmospheric conditions to form the alkoxy radical, CHF_2OCF_2O. This radical may further decompose via the following three reactions.

$$CHF_2OCF_2O \rightarrow CHF_2O + CF_2O \qquad (6)$$

$$CHF_2OCF_2O \rightarrow CHF_2OCOF + F \qquad (7)$$

$$CHF_2OCF_2O + O_2 \rightarrow CF_2O + CF_2O + HO_2 \qquad (8)$$

Reaction 6 results in the formation of CF_2O and CHF_2O and is exothermic by −3.6 kcal mol^{-1}. A barrier height of 10.3 kcal mol^{-1} is predicted to exist. Reaction 7 is a C−F bond-breaking reaction that is endothermic by 18.5 kcal mol^{-1}. Reaction 8 is a hydrogen abstraction reaction mediation by molecular oxygen. The reaction is highly favorable, with a reaction enthalpy of −44.6 kcal mol^{-1} and a barrier height of only 1.7 kcal mol^{-1}.

We find that the atmospheric oxidation of E134 is likely to form carbonyl fluoride from three possible pathways. Reactions 5, 6, and 8 are each thermodynamically plausible pathways that could result in the formation of CF_2O. Experiments were performed to verify some salient aspects of the theoretical

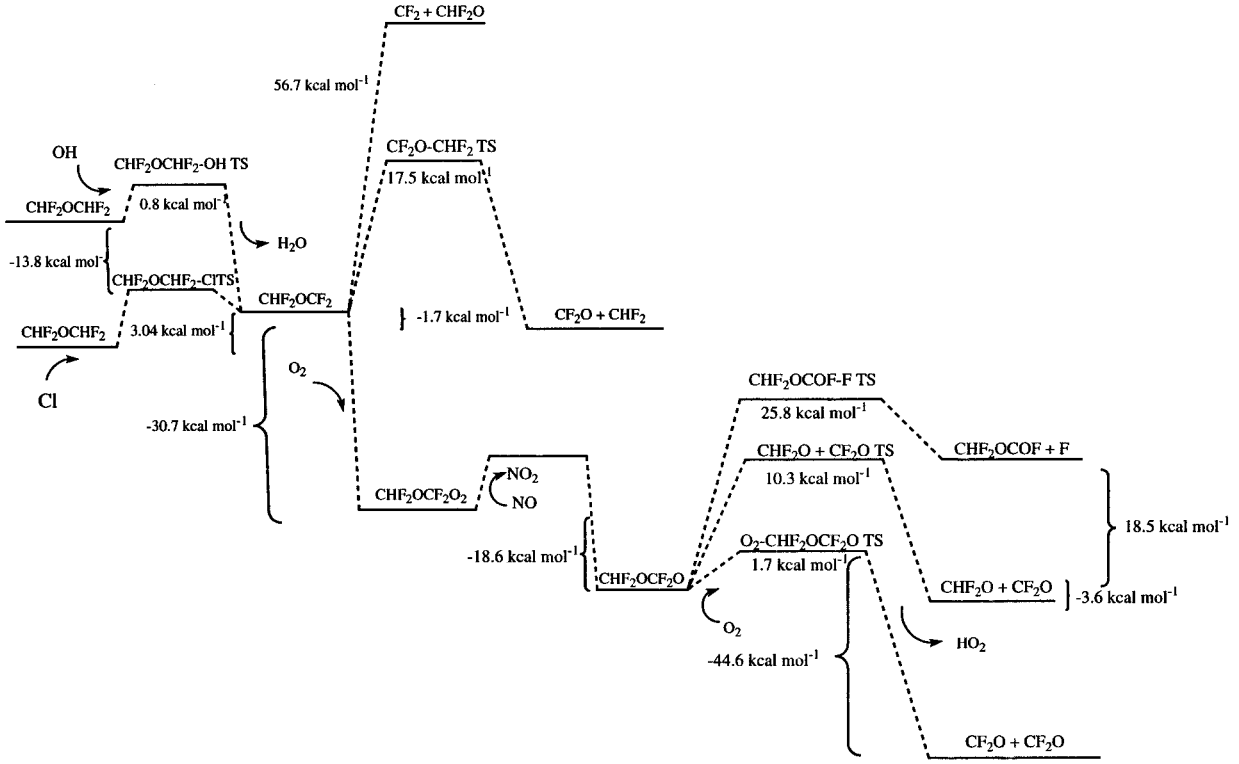

Figure 2. Energy diagram for oxidation of E134.

TABLE 1: Energetics for the Atmospheric Oxidation of E134

reaction	enthalpy (kcal mol^{-1})	activation energy (kcal mol^{-1})
$CHF_2OCHF_2 + OH \rightarrow H_2O + CHF_2OCF_2$	−13.8	0.8
$CHF_2OCF_2 + O_2 \rightarrow CHF_2OCH_2O_2$	−30.7	no barrier
$CHF_2OCF_2 \rightarrow CHF_2 + CF_2O$	−1.7	17.5
$CHF_2OCF_2 \rightarrow CHF_2O + CF_2$	56.7	>56.7
$CHF_2OCF_2O_2 + NO \rightarrow CHF_2OCF_2O + NO_2$	−18.6	
$CHF_2OCF_2O + O_2 \rightarrow CF_2O{-}CF_2O + HO_2$	−44.6	1.7
$CHF_2OCF_2O \rightarrow CHF_2O + CF_2O$	−3.6	10.3
$CHF_2OCF_2O \rightarrow CHF_2OCOF + F$	18.5	25.8

investigation. The objective of the experiments was to verify the predicted products and to determine if the bond-cleaving reaction was indeed feasible under atmospheric conditions. The first experiment consisted of E134, chlorine (both ∼1 Torr), and a large excess of oxygen such that the final pressure was 100 Torr. The only product observed in this reaction was CF_2O. Calibration curves for carbonyl fluoride were generated by reacting difluoromethane (CH_2F_2) with chlorine in a large excess of oxygen. The result of this reaction is the formation of carbonyl fluoride. The decay of difluoromethane in units of molecules per cubic centimeter is plotted against the growth in of carbonyl fluoride in Figure 3. The slope of this line is thus equal to the product of the path length and the absorbance cross section of carbonyl fluoride for that particular absorbance band. Using these data, the decrease in the concentration of E134 can be plotted against the increase in concentration of carbonyl fluoride, as shown in Figure 4. The average yield from three replicate trials is 200 ± 12%. Thus, two molecules of carbonyl fluoride are produced from each molecule of E134 reacted. Quoted errors represent two standard deviations (SDs) about the mean.

A second set of experiments was performed without oxygen; helium was used instead of oxygen to buffer the reaction mixture

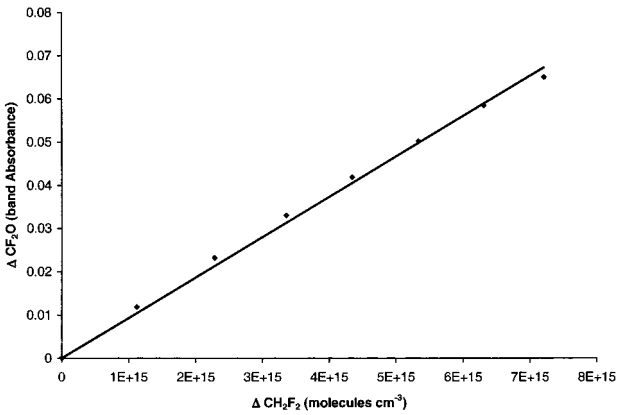

Figure 3. Calibration curve for CF_2O.

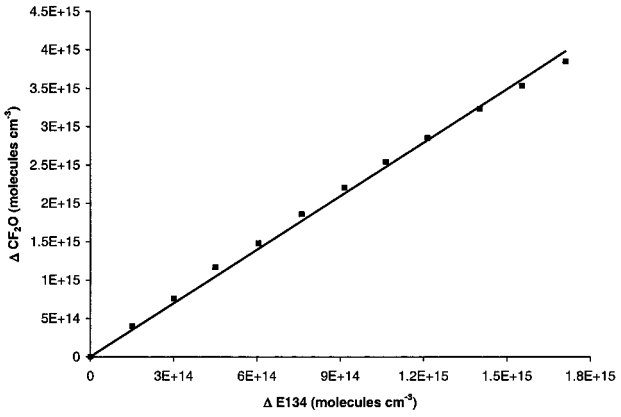

Figure 4. Carbonyl fluoride yield from oxidation of E134.

to 100 Torr. In the absence of O_2, reactions 6 and 8 become impossible and thus any CF_2O formed can be attributed to reaction 5. Significant concentrations of CF_2O were again produced; thus, reaction 5 is feasible at room temperature. In

addition to carbonyl fluoride, products such as CF_2Cl_2 and $CClF_2OCClF_2$ were identified. CF_2Cl_2 is produced from secondary reactions of the CHF_2 fragment formed from reaction 5. $CClF_2OCClF_2$ forms from chlorine addition to the CHF_2OCF_2 radical, which is thus in competition with the fragmentation reaction (reaction 5). In the presence of oxygen, CHF_2 radicals react with excess oxygen to form a second CF_2O molecule per molecule of E134 reacted.

We find that the atmospheric oxidation of E134 is likely to result in the formation of CF_2O via reactions 5, 6, and 8. Ultimately, 2 equiv of carbonyl fluoride will result from the atmospheric oxidation of E134 either directly through reaction 8 or through the further oxidation of CHF_2 and CHF_2O radicals formed in reactions 5 and 6.

Dissociation of the CHF_2OCF_2 radical is shown to be a plausible reaction channel in the oxidation of E134. One consideration concerning the degree of CHF_2OCF_2 fragmentation is the amount of internal energy within the radical formed during the initial hydrogen abstraction reaction. As an example, consider the CF_3CHFO radical formed during the oxidation of HFC134a and studied by numerous investigators.[14−19] The removal of CF_3CHFO occurs via two competing reaction pathways.

$$CF_3CHFO + O_2 \rightarrow CF_3COF + HO_2 \quad (9)$$

$$CF_3CHFO \rightarrow CF_3 + HFCO \quad (10)$$

Reaction 9 is a hydrogen abstraction reaction initiated by molecular oxygen, whereas reaction 10 is a unimolecular dissociation reaction. There are also two ways in which CF_3CHFO radicals can be formed.

$$CF_3CHFO_2 + CF_3CHFO_2 \rightarrow CF_3CHFO + CF_3CHFO + O_2 \quad (11)$$

$$CF_3CHFO_2 + NO \rightarrow CF_3CHFO + NO_2 \quad (12)$$

The RO_2 self-reaction (reaction 11) is exothermic by − 6 kcal mol^{-1}, whereas reaction 12 is exothermic by greater than −17 kcal mol^{-1}. Wallington et al.[19] determined that unimolecular decomposition of CF_3CHFO radicals (reaction 10) was much more important when the CF_3CHFO radicals were produced from reaction 12 rather than reaction 11. They ascribe this observation to the differences in the internal energy of CF_3CHFO resulting from different production mechanisms (reactions 11 and 12). Reaction 11 generated thermalized or ground-state CF_3CHFO radicals, whereas only 36% of the radicals were thermalized in reaction 12. The remaining fraction contained sufficient energy to undergo prompt dissociation.

The CHF_2OCF_2 radical can analogously be produced two different ways; from reaction of E134 with chlorine atoms or with hydroxyl radicals. Our calculations show that with hydroxyl radical, hydrogen abstraction from E134 is exothermic by −13.8 kcal mol^{-1}. However, the experiments were done using chlorine atoms. Good et al.[20] determined the heat of formation of CHF_2OCHF_2 and CHF_2OCF_2 to be −314.5 and −261.0 kcal mol^{-1}, respectively, whereas the heats of formation for Cl and HCl are 28.9 and −22.06 kcal mol^{-1}, respectively. From these data, the hydrogen abstraction reaction initiated by chlorine atoms is calculated to have a thermoneutral reaction enthalpy of 3.0 kcal mol^{-1} (Figure 2). Based on the differences in reaction enthalpies between Cl- and OH-initiated reactions, the amount of CHF_2OCF_2 fragmentation in systems employing OH may be greater than in systems employing Cl atoms.

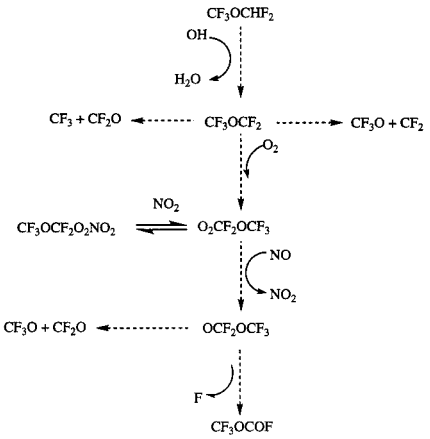

Figure 5. Oxidation mechanism for CF_3OCHF_2 (E125).

TABLE 2: Energetics for the Atmospheric Oxidation of E125

reaction	enthalpy (kcal mol^{-1})	activation energy (kcal mol^{-1})
$CF_3OCHF_2 + OH \rightarrow H_2O + CF_3OCF_2$	−14.1	2.1
$CF_3OCF_2 + O_2 \rightarrow CF_3OCF_2O_2$	−27.1	no barrier
$CF_3OCF_2 \rightarrow CF_3 + CF_2O$	−1.0	18.9
$CF_3OCF_2 \rightarrow CF_3O + CF_2$	60.2	>60.2
$CF_3OCF_2O_2 + NO \rightarrow CF_3OCF_2O + NO_2$	−19.6	
$CF_3OCF_2O \rightarrow CF_3O + CF_2O$	−2.6	9.4
$CF_3OCF_2O \rightarrow CF_3OCOF + F$	18.8	22.8

B. CF_3OCHF_2. The oxidation of E125 is illustrated in Figure 5. The energetics of these pathways are tabulated and illustrated in Table 2 and Figure 6, respectively. The first step in the oxidation of E125 is removal of its sole hydrogen atom by the hydroxyl radical. The barrier for this reaction is calculated to be 2.1 kcal mol^{-1} at the B3LYP/6-311+G(2d,2p)//B3LYP/6-31G(d) level of theory.

$$CF_3OCHF_2 + OH \rightarrow CF_3OCF_2 + H_2O \quad (13)$$

Hsu et al.[10] measured the activation barrier to be 4.2 kcal mol^{-1}, which is 2.1 kcal mol^{-1} higher than our calculated activation barrier. The enthalpy of this reaction is calculated to be exothermic by −14.1 kcal mol^{-1}. Hsu et al.[10] determined a CH bond strength for E125 to be 106.0 ± 1.0 kcal mol^{-1}. Given that the OH bond strength of water is 119.3 ± 1.0 kcal mol^{-1}, the enthalpy of reaction 13 is determined to be −13.3 ± 1.4 kcal mol^{-1}. Our determination of the enthalpy for this reaction is within experimental error of this value.

The CF_3OCF_2 radical formed in the initial reaction may participate in the following removal mechanisms:

$$CF_3OCF_2 \rightarrow CF_3 + CF_2O \quad (14)$$

$$CF_3OCF_2 \rightarrow CF_3O + CF_2 \quad (15)$$

$$CF_3OCF_2 + O_2 \rightarrow CF_3OCF_2O_2 \quad (16)$$

Reactions 14 and 15 are dissociation processes involving the CO bonds of the alkyl radical. As shown in Table 2, reaction 15 is endothermic by >60 kcal mol^{-1} and is therefore unlikely to be of any significance under atmospheric conditions. Reaction 14 is predicted to be exothermic by −1.0 kcal mol^{-1}. In addition, a positive entropy change (0.0381 kcal mol^{-1} K^{-1}) is associated with this reaction, making it spontaneous by −12.4 kcal mol^{-1} at 298 K. Reaction 16 is an O_2 addition reaction forming an

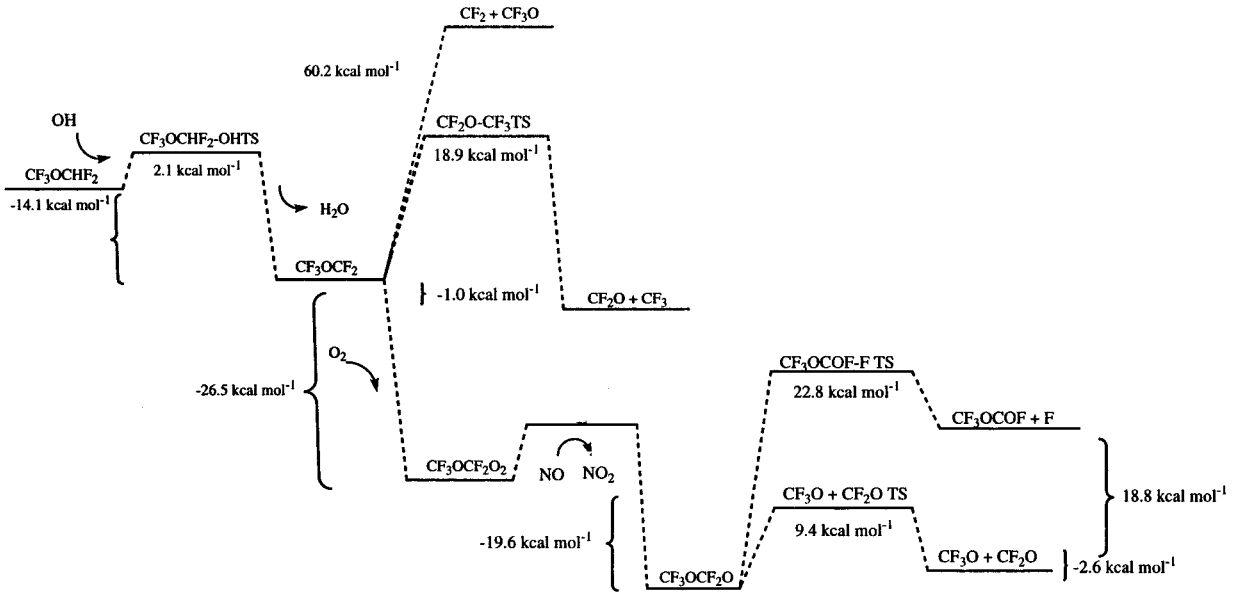

Figure 6. Energy diagram for oxidation of E125.

alkylperoxy radical. The reaction is exothermic by −27.1 kcal mol^{-1}, but the reaction has a negative entropy change (−0.0442 kcal mol^{-1} K^{-1}), making the process spontaneous at 298 K by −13.9 kcal mol^{-1}. As with the analogous reactions in the E134 system, the bimolecular addition reaction (reaction 16) and the bond dissociation reaction producing carbonyl fluoride (reaction 14) are predicted to be almost equally favorable from a thermodynamic perspective. Kinetically, the bimolecular oxygen addition reaction proceeds without barrier, whereas the unimolecular dissociation reaction has a reaction barrier of 18.9 kcal mol^{-1}.

The alkylperoxy radical formed in reaction 16 is reduced under atmospheric conditions to an alkoxy radical as described in reaction 17. The reaction enthalpy for this reaction was −19.6 kcal mol^{-1}.

$$CF_3OCF_2O_2 + NO \rightarrow CF_3OCF_2O + NO_2 \qquad (17)$$

The alkoxy radical formed in this reaction can participate in two bond dissociation pathways as shown by reactions 18 and 19.

$$CF_3OCF_2O \rightarrow CF_3OCOF + F \qquad (18)$$

$$CF_3OCF_2O \rightarrow CF_3O + CF_2O \qquad (19)$$

Reaction 18 involves the cleaving of a C−F bond to form a potentially stable reservoir species, CF_3OCOF. The reaction is, however, highly endothermic, with a reaction enthalpy of 18.8 kcal mol^{-1}, thus making the reaction improbable. Reaction 19 involves the cleaving of a CO bond to form CF_3O and carbonyl fluoride. The reaction is exothermic by −2.6 kcal mol^{-1} and has a modest barrier of 9.4 kcal mol^{-1}.

We find that the atmospheric oxidation of E125 is likely to result in the formation of carbonyl fluoride. Two different reactions can account for the formation of carbonyl fluoride. The first reaction is the dissociation of CF_3OCF_2 to form CF_3 and CF_2O (reaction 14) and the second possibility is the dissociation of CF_3OCF_2O to form CF_3O and CF_2O (reaction 19).

To verify that reaction 14 is indeed possible under atmospheric conditions, analogous experiments to those described previously for E134 were conducted. In the presence of a large excess of oxygen, the only product observed was CF_2O. The

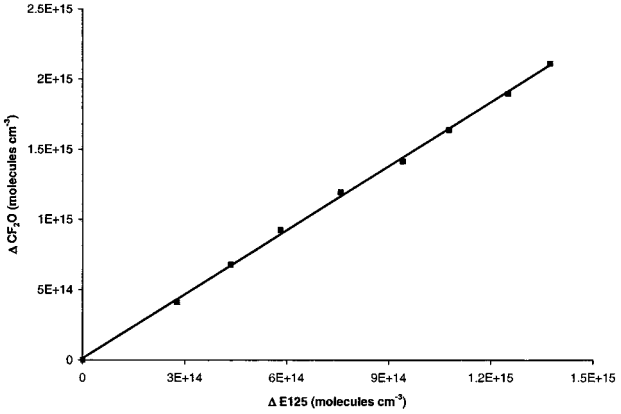

Figure 7. Carbonyl fluoride yield from oxidation of E125.

percent yield for carbonyl fluoride was calculated to be only 152 ± 13% compared with the 200 ± 12% yield determined for E134 (Figure 7). This difference in the yield of carbonyl fluoride is a result of the secondary chemistry of CHF_2O and CF_3O radicals. Under oxygen-rich conditions, the CHF_2O radical formed in the oxidation of E134 is rapidly converted into a second carbonyl fluoride molecule. The CF_3O radical formed from E125 can participate in a C−F dissociation process, resulting in the formation of carbonyl fluoride and F atoms; however, this reaction is slow.[27] In competition with this reaction is the reaction between CF_3O_2 and CF_3O radicals, which results in the formation of CF_3OOOCF_3. The presence of this species has been reported by a number of investigators in association with the atmospheric oxidation of species containing a CF_3 functional group.[16,21−24] Figure 8 is an IR spectrum of CF_3OOOCF_3 recorded during the oxidation of E125 after features due to E125 and carbonyl fluoride have been subtracted. Absorbance maximums measured at 1174, 1257, and 1294 agree well with those reported previously for CF_3OOOCF_3 at 1171, 1254, and 1291 cm^{-1}, respectively. The detection of this species is evidence that suggests the participation of reaction 14 in the overall mechanism. The formation of CF_3OOOCF_3 requires the presence of CF_3O_2 radicals, which are formed from oxygen addition to the CF_3 radicals formed in reaction 14.

The second experiment consisted of the same amount of E125 and chlorine but no oxygen. The pressure was buffered with

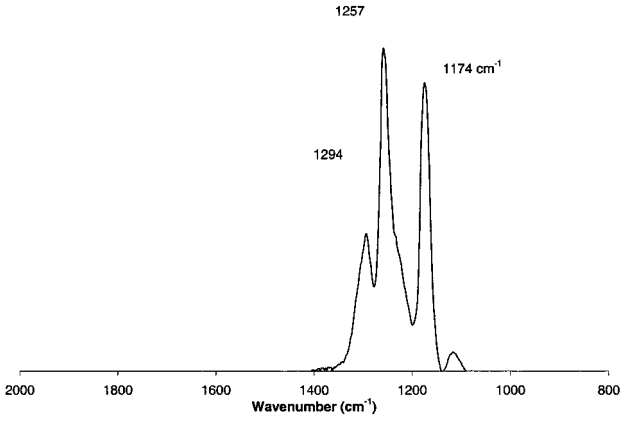

Figure 8. Vibrational spectra for CF_3OOOCF_3.

98 Torr of helium instead of oxygen. In the absence of oxygen, reaction 16 becomes impossible; thus, if any CF_2O is produced it must come from reaction 14. As with E134, E125 produced significant quantities of carbonyl fluoride in the absence of oxygen. In addition to CF_2O, CF_3Cl and CF_3OCF_2Cl were also identified products.

Thus, the atmospheric fate of E125 is predicted to be reaction with OH to form CF_3OCF_2, followed by competition between a CO-dissociation reaction to form CF_3 and CF_2O, and an O_2-addition reaction ultimately forming CF_2O and CF_3O. Under atmospheric conditions, both the CF_3 and CF_3O radicals can be oxidized to another CF_2O molecule via the following mechanisms.

$$CF_3 + O_2 \rightarrow CF_3O_2 \quad (20)$$

$$CF_3O_2 + NO \rightarrow CF_3O + NO_2 \quad (21)$$

$$CF_3O + NO \rightarrow CF_2O + FNO \quad (22)$$

Although the dissociation reaction has been shown both theoretically and experimentally to be possible at room temperature, the relatively large barrier height predicted by our ab initio calculations suggests that the reaction may be slow.

C. CF_3OCH_3. The proposed degradation mechanism for E143a is illustrated in Figure 9. The energetics calculated at the B3LYP/6-311+G(2d,2p)//B3LYP/6-31G(d) level of theory are presented in Table 3 and Figure 10. The initial hydrogen abstraction reaction is predicted to have a barrier of 0.0 kcal mol^{-1}, which is ~3 kcal mol^{-1} lower than the determination of Hsu et al.[10] who measured a barrier of ~3.1 kcal mol^{-1}. Our methodology has consistently underestimated the barrier heights for OH radical reactions by ~3 kcal mol^{-1}.

$$CF_3OCH_3 + OH \rightarrow CF_3OCH_2 + H_2O \quad (23)$$

The enthalpy for reaction 23 is estimated to be ~−17.1 kcal mol^{-1}. Hsu et al.[10] determined the CH bond dissociation energy of E143a to be 102.0 ± 1.0 kcal mol^{-1}. Thus, the reaction of E143a with OH can be estimated from this experimental data to be −17.3 ± 1.4 kcal mol^{-1}. This value compares very well with our ab initio results.

The CF_3OCH_2 radical formed may undergo the following three reactions.

$$CF_3OCH_2 \rightarrow CF_3O + CH_2 \quad (24)$$

$$CF_3OCH_2 \rightarrow CF_3 + CH_2O \quad (25)$$

$$CF_3OCH_2 + O_2 \rightarrow CF_3OCH_2O_2 \quad (26)$$

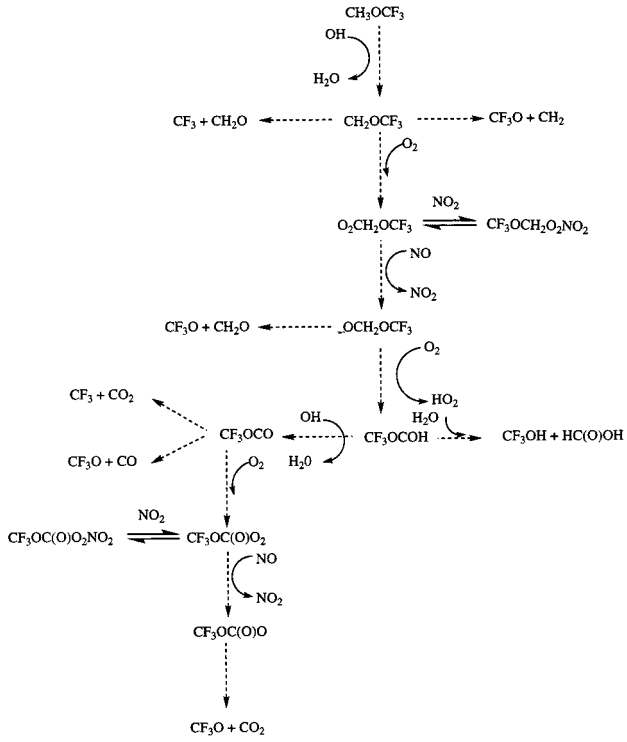

Figure 9. Oxidation mechanism for CF_3OCH_3 (E143a).

TABLE 3: Energetics for the Atmospheric Oxidation of E143a

reaction	enthalpy (kcal mol^{-1})	activation energy (kcal mol^{-1})
$CF_3OCH_3 + OH \rightarrow H_2O + CH_2OCF_3$	−17.1	0.0
$CF_3OCH_2 + O_2 \rightarrow CF_3OCH_2O_2$	−27.4	no barrier
$CF_3OCH_2 \rightarrow CF_3 + CH_2O$	20.2	36.4
$CF_3OCH_2 \rightarrow CF_3O + CH_2$	112.0	>112.0
$CF_3OCH_2O_2 + NO \rightarrow CF_3OCH_2O + NO_2$	−22.5	
$CF_3OCH_2O_2 + NO_2 \rightarrow CF_3OCH_2O_2NO_2$	−17.6	no barrier
$CF_3OCH_2O + O_2 \rightarrow CF_3OCOH + HO_2$	−34.8	7.6
$CF_3OCH_2O \rightarrow CF_3O + CH_2O$	20.6	21.2
$CF_3OCH_2O \rightarrow CF_3OCOH + H$	14.5	19.8
$CF_3OCOH + OH \rightarrow CF_3OCO + H_2O$	−17.0	0.0
$CF_3OCOH + H_2O \rightarrow CF_3OH + HC(O)OH$	−9.7	29.6
$CF_3OCO + O_2 \rightarrow CF_3OC(O)O_2$	−29.1	no barrier
$CF_3OCO \rightarrow CF_3 + CO_2$	−17.9	13.7
$CF_3OCO \rightarrow CF_3O + CO$	15.7	22.1
$CF_3OC(O)O_2 + NO \rightarrow CF_3OC(O)O + NO_2$	−29.1	
$CF_3OC(O)O_2 + NO_2 \rightarrow CF_3OC(O)O_2NO_2$	−21.0	no barrier
$CF_3OC(O)O \rightarrow CF_3O + CO_2$	−8.3	11.9

As shown in Table 3 and Figure 10, reactions 24 and 25 are bond-cleaving reactions involving the CO bonds in E143a. Both reactions are significantly endothermic, with high activation barriers. For E134 and E125, the analogous reactions to reaction 25 were found to be energetically favorable, whereas reaction 25 is considerably endothermic by 20.2 kcal mol^{-1} and is unlikely to compete with the oxygen addition reaction (reaction 26). Reaction 26 is exothermic by −27.4 kcal mol^{-1} and proceeds without barrier. Reaction 26 produces an alkoxy radical, RO_2, that under atmospheric conditions in the presence of NO is reduced to alkoxy radicals, RO. The enthalpy of this reaction is −22.5 kcal mol^{-1}. Alternatively, the RO_2 radical may add nitrogen dioxide to form the peroxy nitrate, $CF_3OCH_2O_2NO_2$. Christensen et al.[28] found this radical to be

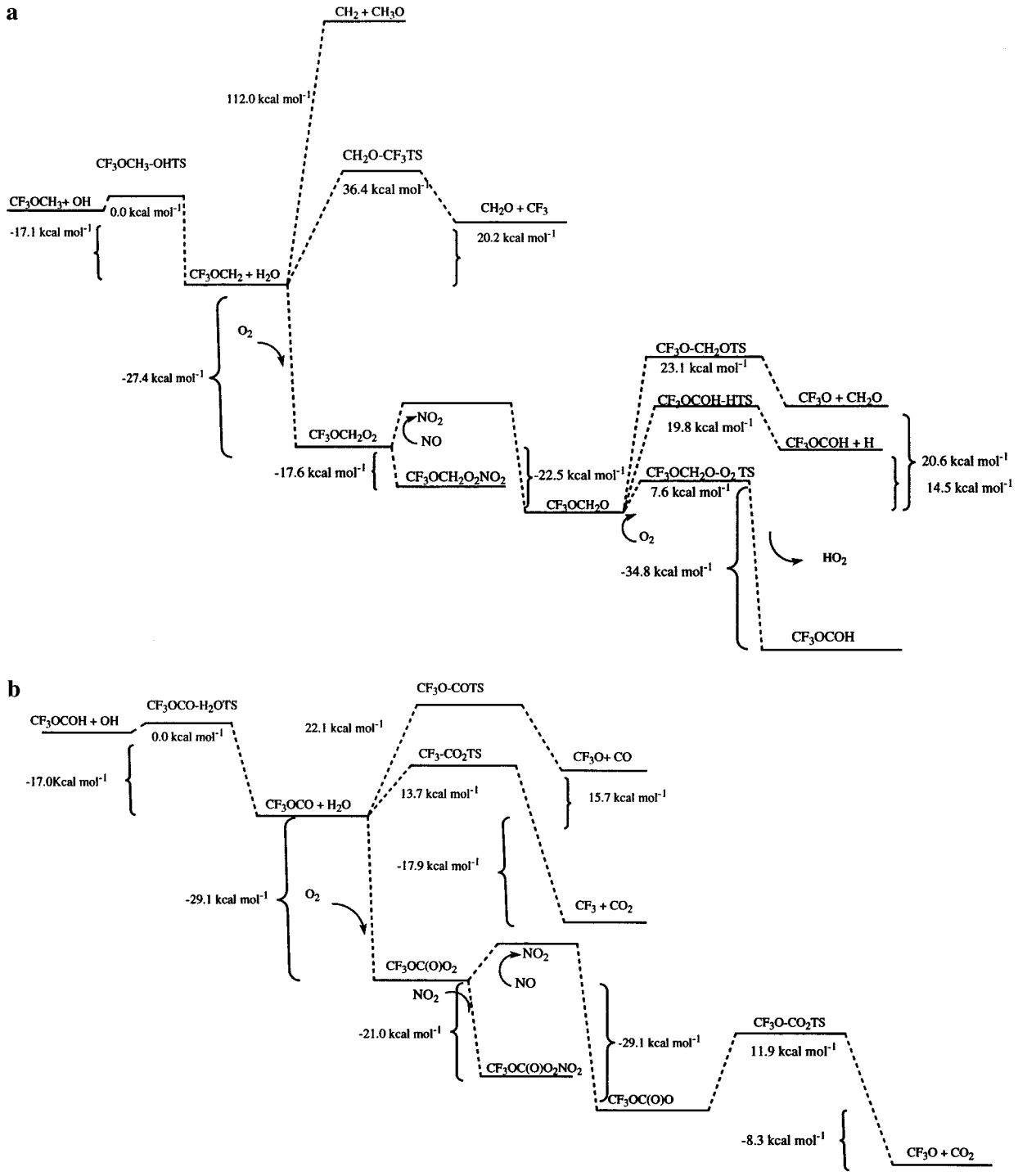

Figure 10. (a) Energy diagram for oxidation of E143a. (b) Energy diagram for oxidation of trifluoromethyl formate, CF_3OCOH.

thermally unstable with respect to the regeneration of NO_2 and $CF_3OCH_2O_2$. Our calculations predict the formation of the alkyl peroxy nitrate species to be exothermic by -17.6 kcal mol^{-1}. This quantity is also the barrier to dissociation of the alkyl peroxy nitrate species.

$$CF_3OCH_2O \rightarrow CF_3O + CH_2O \qquad (27)$$

$$CF_3OCH_2O \rightarrow CF_3OCOH + H \qquad (28)$$

$$CF_3OCH_2O + O_2 \rightarrow CF_3OCOH + HO_2 \qquad (29)$$

The alkoxy radical, CF_3OCH_2O may participate in two bond-cleavage reactions. The first (reaction 27) is a CO bond cleavage resulting in the formation of CF_3O and CH_2O. The second (reaction 28) is a CH bond cleavage resulting in the formation of trifluoromethyl formate (CF_3OCOH) and H atoms. A third possible pathway is a hydrogen abstraction reaction mediated by molecular oxygen (reaction 29). Christensen et al.[28] suggest that reaction 27 was negligible based the absence of CF_2O, which would result from further reaction of the CF_3O radical in the presence of NO. This logic also stipulates that reaction 24 is negligible as well. These experimental observations agree with the thermodynamics predicted for these reactions. Reaction 27 is predicted to be endothermic by 20.6 kcal mol^{-1}. The CH bond-cleaving reaction has a barrier height of 19.8 kcal mol^{-1} and is endothermic by 14.5 kcal mol^{-1}. The entropy for this

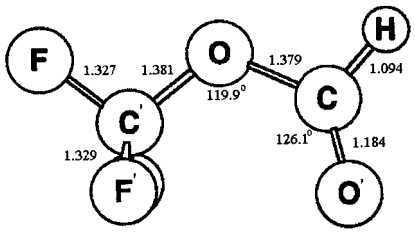

Figure 11. Structure of trifluoromethyl formate.

TABLE 4: Structure of CF_3OCOH[a,b]

coordinate	CF_3OCOH B3LYP/ 6-311++G(3df,3pd)	CH_3OCOH B3LYP/ 6-311++G(3df,3pd)	CH_3OCOH experimental values[c]
C′X	1.327	1.087	1.086
C′X′	1.329	1.090	
C′O	1.381	1.442	1.437
CO	1.379	1.345	1.334
CO′	1.184	1.214	1.200
CH	1.094	1.098	1.101
XC′O	106.7	105.1	
X′C′O	111.8	110.3	
COC′	119.9	114.0	114.8
OCO′	126.1	125.7	125.9
HCO	107.0	108.1	109.3
XC′OC	180.0	180.0	180.0
X′C′OC	61.2	60.4	
O′COC′	0.0	0.0	0.0
HCOC′	180.0	180.0	180.0

[a] Bond lengths in angstroms; bond angles in degrees. [b] X = F, H for CF_3OCOH and CH_3OCOH, respectively. [c] Reference 25.

reaction was estimated to be 23.0 cal mol^{-1} K^{-1}; thus, at 298 K, this reaction is not spontaneous. In contrast, the bimolecular hydrogen abstraction reaction is exothermic by −34.8 kcal mol^{-1}. Based on this analysis, the reservoir species, CF_3OCOH, results predominantly from the reaction of molecular oxygen with CF_3OCH_2O.

For CF_3OCOH, the structure was optimized and a frequency calculation was performed using the B3LYP level of theory and the large 6-311++G(3df,3pd) basis set. The structure of CF_3-OCOH is illustrated and tabulated in Figure 11 and Table 4, respectively. The syn conformer is the more stable conformer, in accord with the work of Wallington et al.[29] Table 4 also contains values for methyl formate for comparison along with experimentally derived values from Curl et al.[25] The structural parameters for methyl formate compare well with the experimental values. There are several structural changes that occur when the three methyl hydrogens in methyl formate are replaced by fluorine atoms to form trifluoromethyl formate. In trifluoromethyl formate, the CO single bonds are of roughly equal length; in methyl formate, the two bonds differ in length by 0.1 Å. The CF_3 group is a highly electron-withdrawing group and thus the CO single bond adjacent to the CX_3 group shortens from 1.442 Å in methyl formate to 1.381 Å in trifluoromethyl formate. Conversely, the opposing CO single bond increases in length from 1.345 to 1.379 Å while the C═O bond decreases in length from 1.214 to 1.184 Å.

The vibrational spectra for trifluoromethyl formate were also calculated at the B3LYP/6-311++G(3df,3pd) level of theory. This method and large basis set is a fairly reliable method for predicting vibrational transitions. In a previous study on the vibrational properties of E143a, E134, and E125 we found the ab initio methodology just mentioned is accurate to within ∼3% of the measured values.[26] The structural model used to describe trifluoromethyl formate assumed C_s symmetry. The 18 normal vibration modes were divided into 13 modes of the A′ representation and six modes of the A″ type; that is,

$$\Gamma_{vib} = 13A' + 6A'' \tag{30}$$

All 18 fundamental modes are allowed and active in both the IR and Raman spectra. The A′ species are symmetric and the A″ species are antisymmetric to the plane of the molecule. Using the band centers and relative intensities calculated from ab initio methods, we simulated an IR spectrum. The simulated spectrum was generated using the calculated frequencies as the mean of a Lorentzian distribution with a full width at half-maximum (fwhm) of 16 cm^{-1}. The Lorentzian is given by the following expression:

$$\frac{1}{\pi}\cdot\frac{\Delta x/2}{(\Delta x/2)^2 + (x-u)^2} \tag{31}$$

where u is the mean or central frequency and Δx is the fwhm.

The tabulated data and simulated spectra are shown in Table 5 and Figure 12, respectively. The simulated spectrum illustrates five intense absorption features in the IR range. The peak at 1854 cm^{-1} is the C═O stretch. The four peaks clustered between 1000 and 1400 cm^{-1} are the CO asymmetric stretch (1103 cm^{-1}) and the three CF stretching modes (1244, 1215, and 1161 cm^{-1}).

Below 800 cm^{-1}, water in the atmosphere absorbs thermal radiation, whereas above 1400 cm^{-1}, water and carbon dioxide both absorb. Therefore, there exists a region between 800 and 1400 cm^{-1} where thermal radiation emitted from the Earth can escape. It is therefore expected that halons with absorption features in this area could contribute to global warming depending on the strength of their absorption features. Trifluoromethyl formate has a band strength of 1580 km mol^{-1}. Good et al.[26] using the same basis set and level of theory determined the total band strength for E143a in the region between 800 and 1300 cm^{-1} to be 1310 km mol^{-1}. Based on this estimate, trifluoromethyl formate may be a stronger radiative forcing agent than the parent species E143a.

Trifluoromethyl formate formed from the oxidation of E143a can be removed by further reaction with hydroxyl radical.

$$CF_3OCOH + OH \rightarrow CF_3OCO + H_2O \tag{32}$$

$$CF_3OCOH + H_2O \rightarrow CF_3OH + HC(O)OH \tag{33}$$

The barrier height for this reaction is estimated to be 0.0 kcal mol^{-1}. Thus, we can estimate that the barrier is on the order of 3 kcal mol^{-1} based on the errors determined previously. The reaction enthalpy is exothermic by −17.0 kcal mol^{-1}. The products of this reaction are the CF_3OCO radical and water. The polarity of CF_3OCOH may allow it to be removed through reaction with atmospheric water vapor or through heterogeneous processes. Reaction of trifluoromethyl formate with water vapor (reaction 33) is predicted to be exothermic by −9.7 kcal mol^{-1}.

The CF_3OCO radical formed in reaction 32 can be removed via three competitive channels: an O_2 addition mechanism and two CO bond cleavage reactions are possible.

$$CF_3OCO \rightarrow CF_3O + CO \tag{34}$$

$$CF_3OCO \rightarrow CF_3 + CO_2 \tag{35}$$

$$CF_3OCO + O_2 \rightarrow CF_3OC(O)O_2 \tag{36}$$

Reaction 34 results in the formation of carbon monoxide and CF_3O radicals. The reaction is endothermic by 15.7 kcal mol^{-1} and is thus unlikely to compete with the remaining two

TABLE 5: Vibrational Assignment of CF_3OCOH

mode symmetry	mode number	description	B3LYP/6-311++G(3df,3pd) frequency[a]	B3LYP/6-311++G(3df,3pd) absolute intensity[b]	exptl frequency[c]	exptl frequency[d]
A′	ν_1	CH stretch	3079	26	2972	
	ν_2	C═O stretch	1854	287	1807	1807
	ν_3	OCH bend	1404	6.14	1384	1377
	ν_4	CF′ stretch	1244	381	1267	1277
	ν_5	CO symmetric stretch	1161	199	1191	1187
	ν_6	CO asymmetric stretch	1103	616	1107	1107
	ν_7	CF_2 symmetric stretch	845	8.0	850	
	ν_8	OCO bend	822	13.1	823	
	ν_9	CF_3 umbrella	582	27.8		
	ν_{10}	CF_2′ bend	550	0.16		
	ν_{11}	CF bend	374	0.6		
	ν_{12}	COC	184	1.0		
A″	ν_{13}	CF_2 asymmetric stretch	1215	363	1245	1246
	ν_{14}	HCO′ wag	1029	0.3	1054	
	ν_{15}	FCF′ bend	621	4.0		
	ν_{16}	CF_3 rock	441	0.53		
	ν_{17}	HCO torsion	213	14.7		
	ν_{18}	CF_3 torsion	91	1.5		

[a] Units of cm^{-1}. [b] Units of km mol^{-1}. [c] This work. [d] Reference 28.

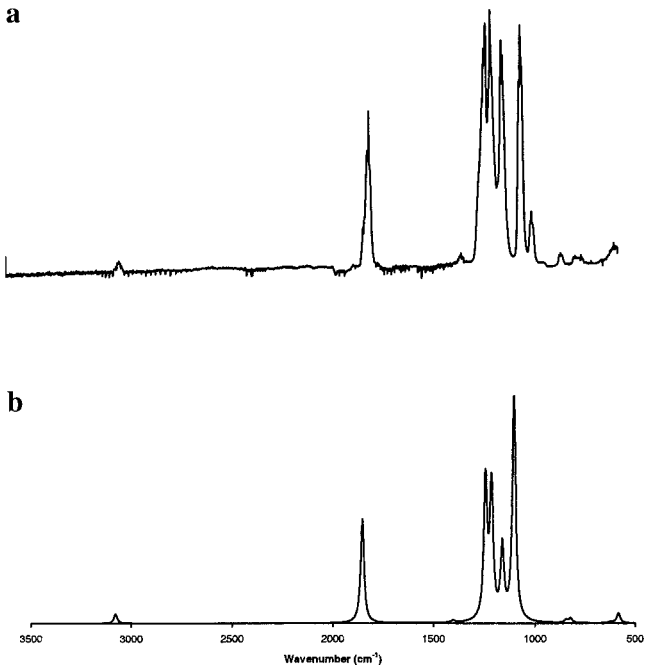

Figure 12. (a) Experimental vibrational spectra of CF_3OCOH. (b) Simulated vibrational spectra of CF_3OCOH.

exothermic processes. Reaction 35 is exothermic by −17.9 kcal mol^{-1} and has a reaction barrier of 13.7 kcal mol^{-1}. Reaction 36 proceeds without barrier and is exothermic by −29.1 kcal mol^{-1}.

The $CF_3OC(O)O_2$ radical formed in reaction 36 is expected to be reduced by NO to form an alkoxy radical, $CF_3OC(O)O$ and NO_2. Alternatively, NO_2 may be added to form $CF_3OC(O)O_2NO_2$, an acyl peroxy nitrate. Christensen et al.[28] observed this species experimentally suggesting that unlike $CF_3OCH_2O_2NO_2$, $CF_3OC(O)O_2NO_2$ is stable with respect to dissociation at room temperature. The reaction enthalpy associated with the formation of $CF_3OC(O)O_2NO_2$ is calculated to be −21.0 kcal mol^{-1} and is thus more stable than $CF_3OCH_2O_2NO_2$, which is in support of the experimental observations.[28]

Ultimately, the $CF_3OC(O)O$ radical decomposes to CO_2 and CF_3O.

$$CF_3OC(O)O \rightarrow CF_3O + CO_2 \qquad (37)$$

Reaction 37 is exothermic by −8.3 kcal mol^{-1} and has a barrier of 11.9 kcal mol^{-1}. Under atmospheric conditions, CF_3O radicals can react with NO to form CF_2O and FNO. Our ab initio calculations suggest that E143a will oxidize to trifluoromethyl formate, CF_3OCOH, and ultimately to carbonyl fluoride and carbon dioxide.

The experimental results are illustrated in Figures 13a−13e. Figure 13a is prior to photolysis and thus only features due to E143a are present. Figure 13b is taken after 9 min of photolysis and shows evidence for the formation of a carbonyl-containing species with an absorption feature at 1807 cm^{-1}. In addition, absorption bands at 1106, 1190, 1245, and 1272 cm^{-1} are visible in the IR spectra. The simulated spectra presented in Table 5 and Figure 12 show the carbonyl stretching mode to resonate at 1854 cm^{-1} in addition to CO and CF stretching modes at 1103, 1161, 1215, and 1244 cm^{-1}. The experimental absorption bands from this work and those of Christensen et al.[28] agree reasonably well with the absorption bands predicted for CF_3OCOH as calculated by ab initio methods. The largest error is ∼2.6%, which is within the error range expected for this ab initio methodology.

At later times in the reaction (Figures 13c and 13d), features due to CF_2O are detectable. Absorption bands at 1944, 1249, 962, and 774 cm^{-1} are evident and have previously been assigned to CF_2O. In addition to CF_2O, carbon dioxide begins to form, and absorption features at 2300 and 667 cm^{-1} are detectable. Also at these times, while features due to CO_2 and CF_2O are increasing, features due to CF_3OCOH are decreasing.

In Figure 13d, features due to CF_3OCOH have decreased substantially while features due to CO_2 and CF_2O continue to grow. Figure 14 illustrates the reaction progress. E143a is shown to decrease continually throughout the reaction. CF_3OCOH is an intermediate that forms at short reaction times, levels off, and begins to decrease at longer reaction times. Both CO_2 and CF_2O emerge at intermediate times and grow substantially throughout the remainder of the reaction. These trends suggest that CO_2 and CF_2O are formed from the further oxidation of CF_3OCOH, which is supported by our ab initio calculations. Additionally, CF_3OOOCF_3 is also detected after subtracting peaks due to carbonyl fluoride. The detection of CF_3OOOCF_3 suggests the participation of reaction 35 in the degradation of E143a. The production of CF_3OOOCF_3 requires the presence of CF_3O_2, which is produced from oxygen addition to CF_3

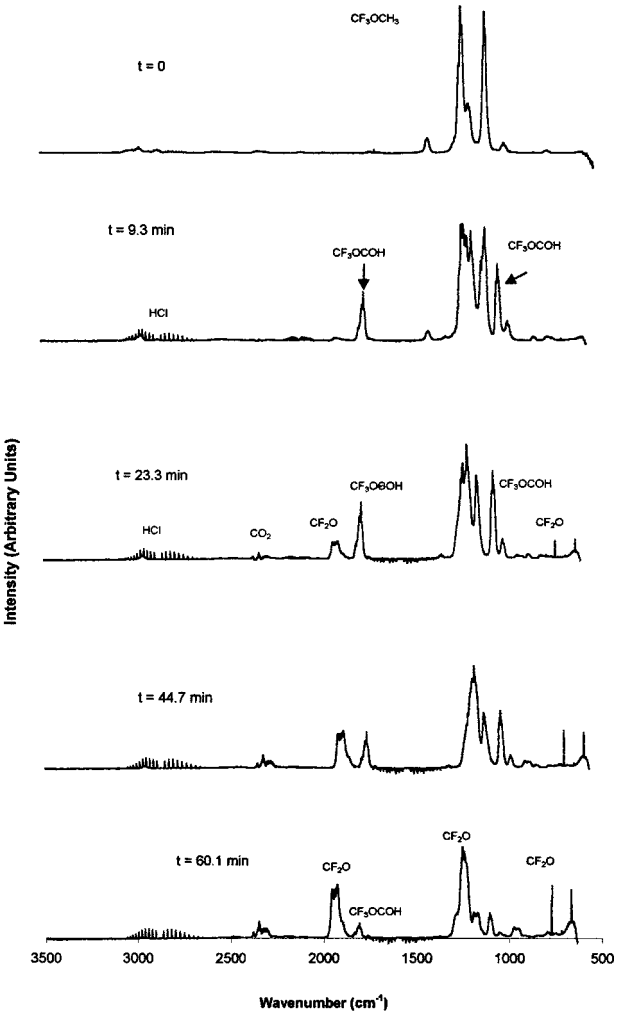

Figure 13. Reaction progress for reaction of E143a with chlorine atoms in the presence of oxygen.

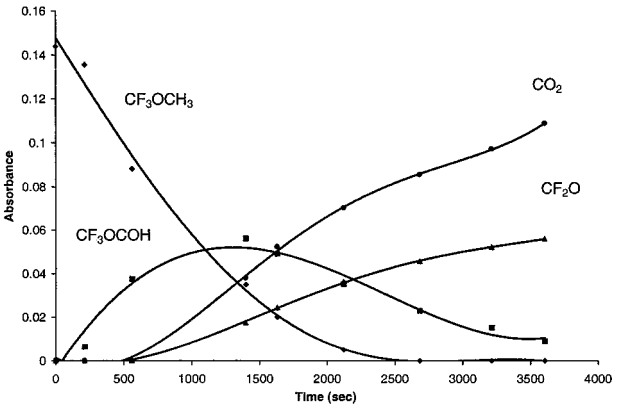

Figure 14. Species concentration as a function of time for the oxidation of E143a.

radicals. Reaction 35 is a thermodynamically plausible source of CF_3 radicals.

IV. Conclusion

E125 and E134 each undergo reaction with tropospheric hydroxyl radical to yield water and an alkyl radical (CF_3OCF_2 and CHF_2OCF_2). The resulting radical can participate in two competitive pathways: reaction with molecular oxygen to yield an alkyl peroxy radical or fragmentation. Under atmospheric conditions, both reactions will result in the formation of two CF_2O molecules per molecule of ether reacted. Both the oxygen addition and bond dissociation pathways are predicted to be energetically favorable. Evidence for the dissociation reaction was found experimentally; however, the substantial barrier height predicted by ab initio calculations suggests that the reaction may be slow compared with the O_2 addition reactions. The oxidation of E143a results in the formation of trifluoromethyl formate (CF_3OCOH). This new reservoir further reacts forming CF_2O and carbon dioxide. In all systems we find evidence for competitions between oxygen addition and bond dissociation reactions.

This work has shown that a major product formed from the oxidation of these fluorinated ethers is carbonyl fluoride. Carbonyl fluoride in the atmosphere is removed rapidly by its heterogeneous reaction with water. This reaction results in the formation of hydrofluoric acid and carbon dioxide. The lifetime of carbonyl fluoride is estimated to be on the order of days.[30]

References and Notes

(1) Calm, J. M.; Didion, D. A. *Tradeoffs in Refrigerant Selections: Past, Present, and Future*; ASHRAE/NIST, Refrigerant Conference, Refrigerants for the 21st Century, Gaithersburg, MD, 1997; Vol. 6.

(2) International Panel on Climate Change (IPCC). *Climate Change 1995: The Science of Climate Change*; Houghton, J. T., Meira Filho, L. G., Bruce, J., Lee, H., Cllander, B. A., Haites, E., Harris, N., Maskell, K., Eds.; Cambridge University Press: New York, 1996.

(3) Pinnock, S.; Hurley, M.; Shine, K. P.; Walington, T. J.; Smyth, T. J. *J. Geophys. Res*. **1995**, *100*, 23227.

(4) Sekiya, A.; Misaki, A. *CHEMTECH* **1996**, *26*, 44.

(5) Adcock, L. Presented at the International CFC and Halon Alternatives Conference, Baltimore, MD, 1991; p 386.

(6) Salivi-Narklede, M.; Wang, B.; Adcock, L.; Hook, W. A. *J. Chem. Thermodyn*. **1992**, *24*, 1065.

(7) Cooper, D. L.; Cunningham, T. P.; Allan, N. L.; McCulloch, A. *Atmos. Environ.* **1992**, *26A*, 1331.

(8) Zhang, Z.; Saini, R. D.; Kurylo, M. J.; Huie, R. E. *J. Phys. Chem*. **1992**, *96*, 9301.

(9) Garland, N. L.; Medhurst, L. J.; Nelson, H. H. *J. Geophys. Res*. **1993**, *98*, 107.

(10) Hsu, K.-J.; Demore, W. B. *J. Phys. Chem*. **1995**, *99*, 11141.

(11) Good, D. A.; Francisco, J. S.; Jain, A. K.; Wuebbles, D. J. *J. Geophys. Res.* **1998**, *103*, 28181.

(12) Frisch, M. J.; Trucks, G. W.; Schlegel, H. B.; Gill, P. M. W.; Johnson, B. G.; Robb, M. A.; Cheeseman, J. R.; Keith, T.; Peterson, G. A.; Montgomery, J. A.; Raghavachari, K.; Al-Laham, M. A.; Zakrzewski, V. G.; Ortiz, J. V.; Foresman, J. B.; Cioslowski, J.; Stefanov, B. B.; Nanayakkara, A.; Challacombe, M.; Peng, C. Y.; Ayala, P. Y.; Chen, W.; Wong, M. W.; Andres, J. L.; Replogle, E. S.; Gomperts, R.; Martin, R. L.; Fox, D. J.; Binkley, J. S.; DeFrees, D. J.; Baker, J.; Stewart, J. P.; Head-Gordon, M.; Gonzalez, C.; Pople, J. A. *Gaussian 94*, Revision D.2; Gaussian, Inc.: Pittsburgh, PA, 1995.

(13) Lee, C.; Yang, W.; Parr, R. G. *Phys. Rev. B* **1988**, *41*, 785.

(14) Wallington, T. J.; Hurley, M. D.; Ball, J. C.; Kaiser, E. W. *Environ. Sci. Technol*. **1992**, *26*, 1318.

(15) Edney, E. O.; Driscoll, D. J. *Int. J. Chem. Kinet*. **1992**, *24*, 1067.

(16) Tuazon, E. C.; Atkinson, R. *J. Atmos. Chem*. **1993**, *16*, 301.

(17) Bednarek, G.; Breil, M.; Hoffmann, A.; Kohlmann, J. P.; Mors, V.; Zellner, R. *Ber. Bunsen-Ges. Phys. Chem*. **1996**, *100*, 528.

(18) Rattigan, O. V.; Rowley, D. M.; Wild, O.; Jones, R. L.; Cox, R. A. *J. Chem. Soc., Faraday Trans*. **1994**, *90*, 1819.

(19) Wallington, T. J.; Frachebouch, J. M.; Orlando, J.; Tyndall, G. S.; Sehested, J.; Mogelberg, T. E.; Nielsen, O. J. *J. Phys. Chem*. **1996**, *100*, 18116.

(20) Good, D. A.; Francisco, J. S. *J. Phys. Chem. A* **1998**, *102*, 7143.

(21) Anderson, L. R.; Fox, W. B. *J. Am. Chem. Soc*. **1967**, *89*, 4313.

(22) Hirschmann, R. P.; Fox, W. B.; Anderson, L. R. *Spectrochim. Acta* **1969**, *25A*, 811.

(23) Thompson, P. G. *J. Am. Chem. Soc*. **1967**, *89*, 4316.

(24) Bierbrauer, K. L.; Chiappero, M. S.; Malanca, F. E.; Arguello, G. A. *J. Photochem. Photobiol., A: Chem.* **1999**, *122*, 73.

(25) Curl, R. F. *J. Chem. Phys*. **1959**, *30*, 1529.

(26) Good, D. A.; Francisco, J. S. *J. Phys. Chem. A* **1998**, *102*, 1854.

(27) DeMore, W. B.; Sander, S. P.; Golden, D. M.; Hampson, R. F.; Kurylo, M. J.; Howard, C. J.; Ravishankara, A. R.; Kolb, C. E.; Molina, M. J. *Chemical Kinetics and Photochemical Data for Use in Stratospheric Modeling Evaluation #12*, January 1997, Jet Propulsion Laboratory, Pasadena, CA.

(28) Christensen, L. K.; Wallington, T. J.; Guschin, A.; Hurley, M. D. *J. Phys. Chem. A* **1999**, *103*, 4202.

(29) Wallington, T. J.; Schneider, W. F.; Sehested, J.; Bilde, M.; Platz, J.; Nielsen, O. J.; Christensen, L. K.; Molina, M. J.; Molina, L. T.; Wooldridge, P. W. *J. Phys. Chem. A* **1997**, *101*, 8264.

(30) Wallington, T. J.; Schneider, W. F.; Worsnop, D. R.; Nielsen, O. J.; Sehested, J.; Debruyn, W. J.; Shorter, J. A. *Environ. Sci. Technol*. **1994**, *28*, 320.